IEEE Access
Multidisciplinary | Rapid Review | Open Access Journal

Date of publication xxxx 00, 0000, date of current version xxxx 00, 0000.

Digital Object Identifier 10.1109/ACCESS.2017.DOI

ILoA: Indoor Localization Using Augmented Vector of Geomagnetic Field

SANGJAE LEE[1], SEUNGWOO CHAE[1], AND DONGSOO HAN.[1]
[1]School of Computing, Korea Advanced Institute of Science and Technology, Daejeon, 34141, South Korea

Corresponding author: Dongsoo Han (e-mail: dshan@ kaist.ac.kr).

This research was supported by the Capacity Enhancement Program for Scientific and Cultural Exhibition Services through the National Research Foundation of Korea (2018X1A3A1068603, 2018R1A2A1A05078018)

ABSTRACT In this paper, we propose a new geomagnetic localization scheme, named ILoA, to address error accumulation and global localization. Global localization is a fundamental problem that determines the initial pose under global uncertainty. Moreover, error accumulation using inertial navigation systems (INS) impacts robustness and drift error, making it challenging to achieve reliable estimation. The magnetic field in indoor space generates a unique signature/anomaly, which can be used as a local feature. Earth's magnetic field can be easily influenced by ferromagnetic material from the indoor environment due to its weak intensity. The magnetic field vector measured by a magnetometer depends on the orientation of the sensor, which we term a direction variant. We devise a novel approach to identify location and heading through the direction-variant augmented vector. Since a magnetic field vector under varying poses can produce many different vectors, the geomagnetic map is trained with the transformation. We present experiments in two testbeds, covering open space, showing that the proposed method using the magnetic field vector is efficient for global localization and accuracy compared with a state-of-the-art approach.

INDEX TERMS heading estimation, indoor positioning, magnetic field anomaly, particle filter, pedestrian dead reckoning

I. INTRODUCTION

Indoor positioning and tracking problems are receiving increasing attention in the Internet of Things (IoT) era. RF fingerprinting localization technique, such as a wireless local area network (WLAN) fingerprinting [1]–[3], is one of most well-known methods that use the received signal strength (RSS). This system exploits existing wireless access points (APs) installed in indoor spaces, and it simplifies the deployment process with no additional cost. The problem is that WLAN-based techniques are insufficient to accurately localize because RSS is prone to be affected by environmental noise such as multipath fading. Moreover, a system with a single sensor suffers from ambiguity of measurement.

The sensor fusion technique addresses single-sensor ambiguity by combining the measurements from multiple sensors. In particular, the pedestrian dead reckoning (PDR) technique with off-the-shelf inertial measurement units (IMUs) in a smartphone is often combined with multiple sensors and achieves high-precision results. PDR is an inertial navigation system (INS) for pedestrians using accelerometers and gyroscope sensors to detect pedestrian steps and directional change. PDR tracks the relative path based on the movement change and estimates three factors [4]: heading direction, footstep, and stride. Stride estimation directly double-integrates acceleration but requires the sensor to be mounted on the body, such as on a shoe [5]. Therefore, it is common to model the stride based on meta-information, such as a map or a person's height. The critical point is that since PDR estimates the relative movement path, it is necessary to use a method for determining the initial position. For example, images [6] or wireless signals (e.g., WiFi) [7], [8] have been used as landmarks for absolute coordinates with a priori knowledge to estimate the initial probability distribution.

Geomagnetism is typically used in GPS/INS techniques to estimate absolute heading. Earth's magnetic field can be expressed as a vector for the magnetic flux density to determine the direction of the azimuth (magnetic north) using an e-compass [9]. The challenge is that it is difficult to find magnetic north due to ferromagnetic materials used in buildings. Although these materials cause local magnetic field anomalies, they are sources of unique features to distinguish different locations. The fingerprinting approach constructs

This article has been accepted for publication in a future issue of this journal, but has not been fully edited. Content may change prior to final publication. Citation information: DOI 10.1109/ACCESS.2020.3029281, IEEE Access

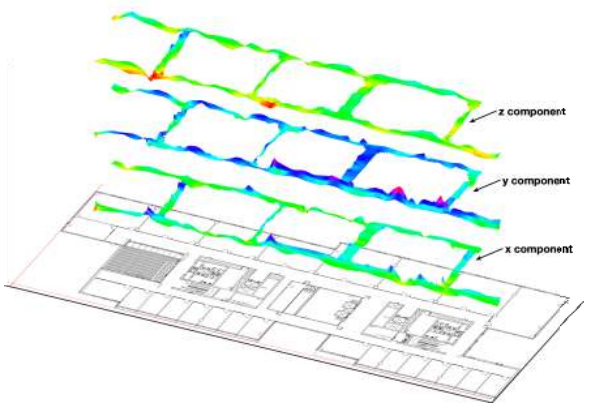

FIGURE 1. Visualization of each axis of the 3D vector of the geomagnetic field in a building

an indoor geomagnetic map, analogous to WLAN fingerprinting. Geomagnetic fingerprinting has distinct advantages, namely, i) no infrastructure requirement, ii) low power consumption, and iii) precise positioning resulting from reliable measurements [10], [11]. Its sampling rate is also noteworthy. The sampling rate of the magnetometer and accelerometer in the category of *micro-electro-mechanical systems* (MEMS) is at least dozens of times faster than WLAN.

The geomagnetic map is a dataset of fingerprints obtained from learning with a priori knowledge of anomalies. The fingerprint contains a magnetic vector, which is a relative value from three orthogonal planes of the magnetometer sensor. Many approaches use the magnitude (ℓ^2-norm) of magnetic vectors instead of using them directly. This magnitude can be categorized as a *direction-invariant* feature from a three-axis magnetometer. These approaches suffer from the global localization problem. The direction-invariant features mean that it is challenging to find the heading direction. Those features usually require the initial distribution of positioning from other sensors or techniques such as a map matching. If we manually determine the initial state, a localization system will not be practical since it would operate only in the constrained start location. Furthermore, there remains the problem of error accumulation because there is no measure to compensate for the absolute heading's drift.

In this paper, we propose a method named ILoA ('I'ndoor 'Lo'calization using 'A'ugmentated Vector of Geomagnetic Field) that fully utilizes the three-dimensional magnetic field illustrated in Fig. 1. We achieve *direct-variant* magnetic features that minimize the information loss by data augmentation. Based on the particle filtering and Markov chains, we obtain the solution of latent variables by recursive Bayesian inference. We design the features encoded in the direction of movement and the path stored in the training phase and then restore them from the proposed augmented feature framework. The proposed method successfully estimates the direction by minimizing the discrepancy between online measurements and offline data. We present a space-division approach based on the alpha shape for optimization of training, allowing optimal resampling for convergence of the particle filter. The space division increases localization performance by reducing the calibration cost and guiding the interpolation area.

The contribution of this paper is as follows.

- This paper proposes a new model of the geomagnetic map to address *the global localization* problem, namely, finding the location at any starting location and heading. The proposed model of the geomagnetic map is designed to minimize information loss.
- This paper proposes a practical methodology to address error accumulation with the *direction-variant* feature. The direction-variant feature corrects the heading orientation and the location. We validate that the direction-variant feature is more effective in an environment where there is with no structural objects, such as open space.
- This paper proposes a new space-division approach to reduce calibration costs and improve the geomagnetic map quality. The approach provides a semi-automated calibration procedure for creating the layout of navigation space on the map and for map matching to improve localization performance.

II. RELATED WORK

The methods of utilizing a magnetic field for positioning can be categorized into two distinct groups: i) a group that exploits additional hardware (such as permanent magnets [12] or coils [13]–[15]) to induce magnetic fields as evidence and ii) a group with no additional hardware using existing infrastructure, such as fingerprinting. Fingerprinting-based localization algorithms use magnetic anomalies caused by ferromagnetic material in buildings. The methods require an indoor environment database, i.e., a geomagnetic map, instead of the special-purpose hardware deployment. To construct a magnetic field map, Chung et al. [16], [17] used specially designed equipment, and Qiu et al. [5] used feet-attached sensors for precise PDR estimation.

Most research studies have utilized the magnitude of the magnetic field, such as the ℓ^2-norm [11], [18]–[22]. Gozick et al. [19] demonstrated the room-level positioning application of smartphones. They analyzed the anomalies and characteristics [23] of the magnetic field in detail. The anomalies due to distortions in an indoor environment are position-specific. Since the magnetic field is affected by the indoor structure, it is stable over time unless there is a structural change [11], [19].

The others can be understood as extracting components from the magnetic field, such as the magnetic inclination angle [18], [24], [25]. Afzal et al. [18] focused on improving the performance of heading estimation using magnetic fields. In this regard, four multiple-input parameters were leveraged, including the norm, two orthogonal planes, which are composed of vertical and horizontal (VH) with an inclination angle. Interestingly, they focused on heading estimation via

high-dimensional feature space. The weight of the input data based on the fuzzy reference was determined. Xie et al. [24] focused on a robust and precise positioning system, named MaLoc, in smartphone applications under different conditions, such as shaking.

Most current studies have also applied three axis values to represent a magnetic feature. Jang et al. [26] and Bae et al. [27] set reference points on the grid of a testbed and then collected magnetic field value vectors from Android smartphones on those points to construct a geomagnetic field map. They generated training and testing sequences of magnetic vectors from the constructed map. They used recursive neural networks (RNNs) for sequence matching and achieved a mean accuracy of approximately 1 meter. Wang et al. [28] also used three-axis geomagnetic vectors with light intensity data. They achieved an accuracy of 1.08 m in the lab and 1.46 m in a corridor with long short-term memory (LSTM). Ashraf et al. [29] proposed MINLOC using a convolutional neural network (CNN) on magnetic patterns (MPs), and they achieved a 1 m distance error. Those studies all employed advanced pattern-matching algorithms to obtain higher precision. However, they had the disadvantage of learning various paths in a two-dimensional space due to time-varying sequence learning. For example, unlearned sequences such as diagonal or other arbitrary movements in a two-dimensional space, such as an open space, cannot be reflected.

In robotics, Kim et al. [25] designed an indoor mobile robot to facilitate floor planning and survey for the geomagnetic map. The mobile robot equipped six arrayed magnetometers, proximity sensors and odometries. They proposed a direction information map, similar to Xie et al. [24] VH components, as a feature integrated into simultaneous localization and mapping (SLAM). The direction information map represents the included angle ($\arctan$), where $[-\pi/2, \pi/2]$, between the X and Y components of the magnetic field in the horizontal plane. Because the sensor is mounted on the robot with a calibrated odometer, they obtained localization results with consistent accuracy.

The problem of the direction-invariant feature, such as a VH or magnitude component, is missing information caused by conversion to scalar, and it has the inherently self-handicapped estimates. That is, the tradeoff reduces the accuracy instead of improving adversarial robustness through the invariant feature with varying orientations. The direct use of a magnetic field vector is a challenging problem where the measurements are taken in directional open form. This means that the magnetic flux density in a sensor's reference frame can be generalized to describe a vector measurement only after the sensor's heading orientation is determined. We suggest a novel method that allows user orientation to be determined by an augmentation of the magnetic field vector. The geomagnetic map is constructed with the orientation to generate the candidates, the augmented magnetic vectors, and we use the similarity measure for candidate pruning.

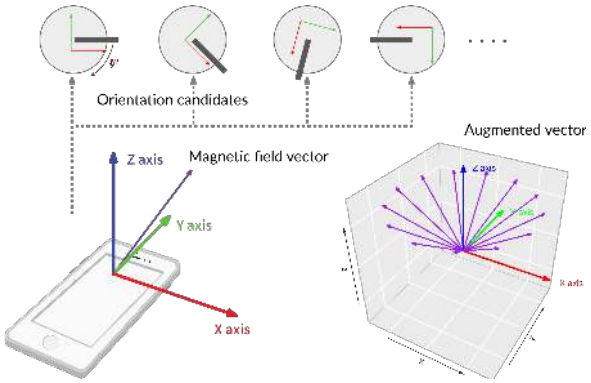

FIGURE 2. Vector augmentation to measure similarity using the magnetic field map

III. METHOD

A. INDOOR GEOMAGNETIC MAP CONSTRUCTION

The geomagnetic map $\mathbb{M}$, which represents the training data on geomagnetic flux anomalies, is a set of geomagnetic fingerprints. The magnetic flux is usually represented by a vector field with the symbol $\vec{B}$. The measured magnetic field vector $\vec{B}$ is expressed by three parameters $[m^x, m^y, m^z]$ in Cartesian space. The fingerprint $\mathbf{f}_l$ is an element of $\mathbb{M}$ as a feature vector, where each feature describes local anomalies $\mathbf{m}_l = [m_l^x, m_l^y, m_l^z]^\intercal$ and specifies a coordinate $\mathbf{c}_l = c_l^x, c_l^y$, where l denotes the location index in the size range from 1 to L with the total number L of reference points. The collecting and labeling procedure for fingerprinting is usually called the offline phase.

The proposed geomagnetic map is designed to augment the feature vector by different orientations, which are estimated using an accelerometer and gyroscope. We define the augmented vector that is produced by transforming a vector to another coordinate frame. Fig. 2 depicts the concept of the augmented vector with purple lines. In the offline phase, we store the orientation using the accelerometer and gyroscope to measure feature similarity at the localization (online) phase.

The orientation is represented by (ϕ, θ, ψ), which denotes roll, pitch, and yaw (azimuth) from the smartphone, respectively. The fingerprint $\mathbf{f}_l$, therefore, learns an orientation and the magnetic field:

$$\mathbf{f}_{l\in[1,\dots,\mathrm{L}]} = [c_l^x, c_l^y, m_l^x, m_l^y, m_l^z, \phi_l, \theta_l, \psi_l] \quad \forall \mathbf{f}_l \in \mathbb{M}. \tag{1}$$

After collecting training data, the calibration process is decomposed into two steps to refine the geomagnetic map: i) alignment of the magnetic field vector to unify the coordinate basis into a world frame and ii) regularization of the training data. The world frame is in this paper defined as a conceptual reference, which is used to express the magnetic field vector in a navigation space. The geomagnetic map is transformed, in which

$${}_w\mathbf{m}_l = R_z(\psi)R_y(\theta)R_x(\phi)\,{}_\alpha\mathbf{m}_l \quad \forall l \in [1, \mathrm{L}], \tag{2}$$

This article has been accepted for publication in a future issue of this journal, but has not been fully edited. Content may change prior to final publication. Citation information: DOI 10.1109/ACCESS.2020.3029281, IEEE Access

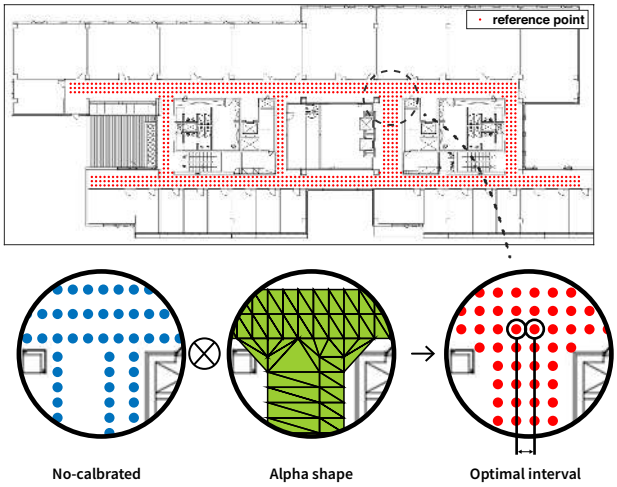

FIGURE 3. The reference points as training data for fingerprinting localization are represented by blue (non-calibrated) and red dots.

where a prescript w, α denotes the world frame and the body (local) frame. For example, the magnetic field vector ${}_w\mathbf{m}$ is a vector in the world frame.

The rotation matrix A performs the coordinate transformation using the following equation:

$$R_z(\psi)R_y(\theta)R_x(\phi) = A(\phi,\theta,\psi) = \begin{bmatrix} \cos\psi & -\sin\psi & 0 \\ \sin\psi & \cos\psi & 0 \\ 0 & 0 & 1 \end{bmatrix} \begin{bmatrix} \cos\theta & 0 & \sin\theta \\ 0 & 1 & 0 \\ -\sin\theta & 0 & \cos\theta \end{bmatrix} \begin{bmatrix} 1 & 0 & 0 \\ 0 & \cos\phi & -\sin\phi \\ 0 & \sin\phi & \cos\phi \end{bmatrix}, \tag{3}$$

where the subscript (x, y, z) denotes rotation around the basis axis.

To regularize the degree of resolution within the training data, we propose an interpolation based on granularity adjustment. We divide an indoor space into two regions by the layout. The inbound is the target area, where localization is required. The rest of the map area is where it is outbound for localization, and no training data are needed. This layout has two aids. In the offline phase, the layout determines whether to generate or filter out references in interpolation. Additionally, to reduce the computation cost in the online phase, this criterion facilitates calculating localization probability using neighboring reference points.

To draw the layout of the indoor space, an alpha shape [30]–[32] is used, and the planning cost is reduced by generalization. Typically, the reference locations where it is set on the floor plan are not always fixed because they depend on the indoor structure and personal tendency, such as expertise and experience. The alpha shape algorithm can cluster a set of nodes as a polygon shape. We consider reference points as the input node set, and a layout of the target area can be achieved through the alpha shape algorithm in Fig. 3.

Fig. 3 shows references (red dots) interpolated based on the raster pattern in the alpha shapes (green polygons). In the alpha shape, the solid lines represent the edges between adjacent points.

Figure 4 in the offline phase represents the floor plan process of how the target region is configured using the alpha shape for a building environment.

1) Collect sensor data at reference points in the target area with the floor plan.
2) Generate polygon nodes via the alpha shape algorithm with the locations of reference points as input nodes.
3) Generate points for the references making a grid structure in the alpha shape polygon.
4) Generate sensor data by interpolation based on the alpha shape polygon.

We propose a *walking survey* (WS) as a site survey to construct the geomagnetic map (step 1 of the floor plan), making it suitable for large-scale space. In mapping, the indoor geomagnetic field map, the method of presetting the start and endpoint of the walking path, aka IndoorAtlas [33] or war walking, has inspired many related studies. The proposed WS method is also based on the walking path. The names of the survey method may vary, but many studies use a mobile collection method that minimizes the calibration effort. Because of this, the conventional manual labeling (ML) procedure for collecting training data is a straightforward survey approach, but it is labor intensive and difficult to deploy in a large-scale site.

We describe the process of resampling and interpolating the WS dataset in pseudocode form Algorithm 1. The floor plan and survey paths are designed before WS, and users collect data while walking with smartphone sensors. The dataset consists of raw data from the accelerometer, gyroscope, and magnetometer. The dataset is resampled on the step rate, tilting, and path direction in postprocessing.

We determine a granularity of interpolation for the fingerprinting calibration as the smallest distance δ from each reference in a grid structure. If we define the magnetometer sampling rate as 20 ms, the sensor's frequency is 50 Hz. If we consider the human gait sampling rate to be approximately 1 s, we can obtain approximately 50 magnetometer samples in a step. If the length of the step stride is 60-70 cm, the magnetometer samples are aligned along with the path plan as reference points spacing every 1.3 cm with a person walking, and $\delta_{\mathbf{m}}$=1.3 cm denotes the distance interval of the magnetometer samples. For example, a WiFi module with a sensing frequency of 10 seconds can construct a δ_{RSS}=6.5 m granularity RSS fingerprint. If we define the optimal granularity solution $\hat{\delta}$ that performs best, the granularity solution $\hat{\delta}$ should be based on satisfying $\delta_{\mathbf{m}} \leq \hat{\delta}$. This is because $\delta_{\mathbf{m}}$ is the maximum possible resolution when using WS.

B. LOCALIZATION WITH AUGMENTED FEATURE VECTOR

ILoA's schematic method of localization is shown in Figure 4. We use Madgwick's attitude and heading reference system (AHRS) [34] orientation algorithm to compensate for

This article has been accepted for publication in a future issue of this journal, but has not been fully edited. Content may change prior to final publication. Citation information: DOI 10.1109/ACCESS.2020.3029281, IEEE Access

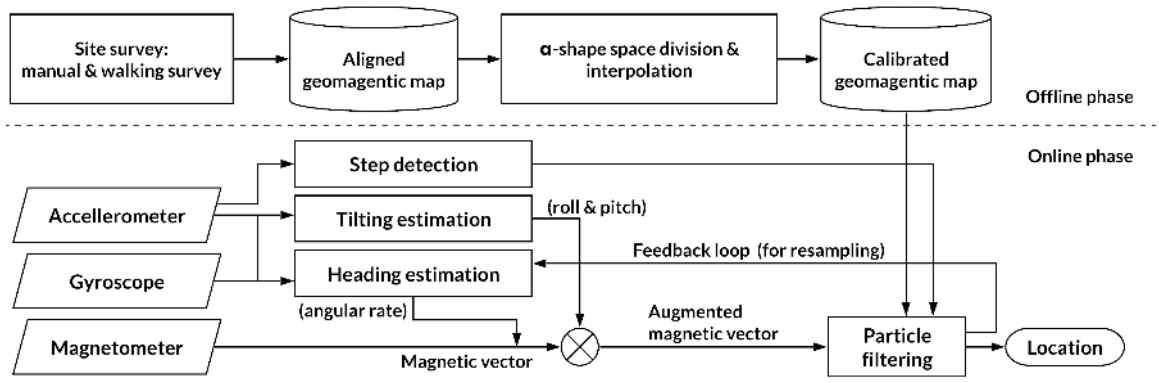

FIGURE 4. Proposed geomagnetic field-based localization scheme.

Algorithm 1: Pseudocode of walking survey

Data: $\mathbb{S}$: measurement datasets, $\mathbb{P}$: corresponding path
Result: $\mathbb{M}$: geomagnetic map
Create paired dataset $\mathbb{D} = \{(\mathbb{S}_1, \mathbb{P}_1), ...)\}$;
for $i := 1$ *to* $|\mathbb{D}|$ **do** *Iteration loop of path*
  Generate resampled $\mathbb{D}'_i$ with a sampling rate λ ;
  Estimate steps using an accelerometer with $\mathbb{D}'_i$;
  Compute timestamp t of step with $\mathbb{D}'_i$;
  Generate interpolated coordinates c with $\|s_i, e_i\|, |t|$;
  for $j := 1$ *to* $|t| - 1$ **do** *Iteration loop of step*
    Generate interpolated coordinates c' with $\|c_j, c_{j+1}\|, (t_{j+1} - t_j)/\delta)$;
    Estimate tilting using an accelerometer and gyroscope with $\mathbb{D}'_i$;
    Compute rotation matrix R with tilt and c' ;
    Generate transformed $\widetilde{\mathbb{D}}'_i$ using $\mathrm{R}^\intercal$;
    Generate $\mathbb{M}_j$ by label c' and interpolation $\widetilde{\mathbb{D}}'_i$;
  end for
  Merge $\mathbb{M}_1, \mathbb{M}_2, ...$ into $\mathbb{M}$;
end for

the noise from the user's handheld device and estimate the accurate tilt and yaw rate. To detect the pedestrian step, the peak detection algorithm is involved in the PDR module. To find the solution of the state, which contains the location and heading, we estimate the rotation matrix as a factor to compare the offline and online measurements. The rotation matrix is composed of the tilt and yaw, which are estimated from the accelerometer and gyroscope.

We present the particle filter for sensor fusion to cover estimated results from multiple sensors. Sensor fusion techniques [35]–[37] are commonly used to solve pedestrian dynamics in probabilistic models, and a sum of random variables approximates the estimated location distribution from multiple independent sensors. The sensor fusion can be expressed as a conditional probability such as the Bayesian filter [38], [39] and modeling latent variables based on hidden Markov models (HMMs) such as position, velocity, and direction, which are indirect measurements. The Kalman filter type of Bayes filters is efficient and widely known for its low computational cost and high accuracy. However, it has two inherent limitations: the estimated probability distribution is limited to a Gaussian distribution, and a linear system is assumed. An extended Kalman filter or an unscented Kalman filter with nonlinearity has been developed, but the assumption of a Gaussian distribution remains a constraint [40]. When tracking a pedestrian, the issue is that the probability distribution is more akin to that of a multivariate Gaussian mixture model. Particle filters are well suited for these two problems, even at higher computational complexity, by approximating any distributions using the concept of particles. Generally, the utilization of more particles provides more satisfactory results.

The particle filter represents the position probability distribution as the sum of the weights of the N particles following:

$$X_k \sim \frac{1}{N}\sum_{i=1}^{N} p\left(\mathbf{x}_k^{[i]}\right) \\ p(\mathbf{x}_k \in X_k) \approx p(\mathbf{x}_k|\mathbf{z}_{1:k}, \mathbf{u}_{1:k}), \tag{4}$$

where $\mathbf{x}$ denotes the state vector of particle $[o^x, o^y, \eta]^\intercal$, $\mathbf{z}$ denotes online measurements that contain tilt $[\phi, \theta]$ and magnetic field vector $\mathbf{b} = [b^x, b^y, b^z]^\intercal$ measurements, and $\mathbf{u}$ denotes human dynamics (step length, yaw rate) $[s, \Delta\psi]$.

The probability distribution of each particle is described by the following equation:

$$p\left(\mathbf{x}_k|Z_k, U_k\right) \\ \propto \underbrace{p(\mathbf{z}_k|\mathbf{x}_k)}_{\text{sensor model}} \left(\int \underbrace{p(\mathbf{x}_k|\mathbf{u}_k, \mathbf{x}_{k-1})}_{\text{motion model}} \right. \\ \left. \underbrace{p(\mathbf{x}_{k-1}|Z_{k-1}, U_{k-1})}_{\text{prior}} \mathrm{d}\mathbf{x}_{k-1} \right), \tag{5}$$

This article has been accepted for publication in a future issue of this journal, but has not been fully edited. Content may change prior to final publication. Citation information: DOI 10.1109/ACCESS.2020.3029281, IEEE Access

where Z_k is all measurements denoted $Z_k = \{\mathbf{z}_i \mid i = 1, ..., k\}$ up to the kth measure and U_k is all actions up to k denoted $U_k = \{\mathbf{u}_i \mid i = 1, ..., k\}$.

The initialization of the state of $p(\mathbf{x}_0)$ involves a uniform distribution, and all particles should have independent heading variables with sufficient diversity. We set the coordinate system that the magnetic field vector collected during the offline phase as the world frame. The online magnetic measurement $\mathbf{b}$ in the online phase is augmented by using the state of particles and converted into the world frame. The augmented vector is illustrated as purple in Fig. 2, which is created by the state of the particle.

The state transition model of a particle is given by the human dynamics following (6):

$$\begin{bmatrix} o'^x \\ o'^y \\ \eta' \end{bmatrix} = \begin{bmatrix} o^x \\ o^y \\ \eta \end{bmatrix} + \begin{bmatrix} (s + \epsilon_s) \cdot \cos(\eta + \Delta\psi + \epsilon_\psi) \\ (s + \epsilon_s) \cdot \sin(\eta + \Delta\psi + \epsilon_\psi) \\ \epsilon_\eta \end{bmatrix}, \quad (6)$$

where s denotes the step length with the particles move; and $\Delta\psi$ is the accumulated yaw change; and ϵ is noise. η is the value that compensates for the drift and determines the heading, which is the direction of particles that should be moved during the kth time. The meaning of η is the heading (yaw) offset converged by the augmented magnetic vector, which is supposed to be transposable to the azimuth by aligning the map coordinate system to the world frame, where the tilt (ϕ, θ) is used to transform the online magnetic vector into a plane horizontally aligned on the ground plane.

The moved particles are sampled after updating the weights of the probabilities. The weight update in the sensor (observation) model (7) is proportional to the similarity measure and is written as follows:

$$\begin{aligned} &p(\mathbf{z}_k|\mathbf{x}_k) \approx \\ &\quad w_k = w_{k-1} p\left(\mathbf{z}_k|\mathbf{x}'_k\right) \propto \frac{1}{f\left(\mathbf{z}_k, \mathbf{x}'_k, \mathbb{M}\right)}, \end{aligned} \quad (7)$$

where $\mathbf{x}'_k$ is the particle state derived from the prediction at time k.

The location likelihood probability of each particle with the kth state $p(\mathbf{z}_k|\mathbf{x}_k)$ is derived from the scoring function f:

$$f\left(\mathbf{z}_k, \mathbf{x}'_k, \mathbb{M}\right) = |[R_z(\eta')A(\phi_k, \theta_k, \Delta\psi_k)^\intercal]_\alpha \mathbf{b}_k - \mathbf{m}_{\mathtt{NN}}|, \quad (8)$$

where ${}_\alpha\mathbf{b}$ is the online magnetic vector in the body frame. Let

$$A(\phi_k, \theta_k, \Delta\psi_k)^\intercal = \begin{bmatrix} a & b & c \\ d & e & f \\ g & h & i \end{bmatrix}.$$

Then, the augmented vector is as follows:

$$\begin{aligned} &[R_z(\eta')A(\phi_k, \theta_k, \Delta\psi_k)^\intercal]_\alpha \mathbf{b}_k = \\ &\left(\begin{bmatrix} \cos\eta & -\sin\eta & 0 \\ \sin\eta & \cos\eta & 0 \\ 0 & 0 & 1 \end{bmatrix} \begin{bmatrix} a & b & c \\ d & e & f \\ g & h & i \end{bmatrix} \right) \begin{bmatrix} b_x \\ b_y \\ b_z \end{bmatrix}. \end{aligned} \quad (9)$$

Each state of particles is provided the tilt (ϕ, θ) and yaw rate $(\Delta\psi)$ to determine A. Let ${}_w\mathbf{b} = ({}^\alpha_w R)\,{}_\alpha\mathbf{b}$, where ${}^\alpha_w R$ is the solution of the rotation matrix that represents the rotation matrix from the local to world frame; then, the augmented vector is as follows:

$$\begin{aligned} {}_w\mathbf{b}_k{}^\intercal = [&(a\cos\eta - d\sin\eta)b_x + (b\cos\eta - e\sin\eta)b_y \\ &+(c\cos\eta - f\sin\eta)b_z, \\ &(a\sin\eta + d\cos\eta)b_x + (b\sin\eta + e\cos\eta)b_y \\ &+(c\sin\eta + f\cos\eta)b_z, \\ &gb_x + hb_y + ib_z]. \end{aligned} \quad (10)$$

We can reduce heading estimation to a rotation matrix optimization problem that finds a transform matrix to the world frame using augmented vector (10).

$$\begin{aligned} \mathtt{NN} &= \arg\min_{l \in L} d(\mathbf{o}, \mathbf{c}_l) \\ d(\mathbf{o}, \mathbf{c}_l) &= \|\mathbf{o} - \mathbf{c}_l\|_2 = \sqrt{\textstyle\sum_{i=x,y}(o^i - c^i_l)^2}. \end{aligned} \quad (11)$$

In (11), the index $\mathtt{NN}$ is noted as the nearest neighbor in $\mathbb{M}$, which is derived from Euclidean distance.

$\mathbf{m}_{\mathtt{NN}}$ is a magnetic field vector in the geomagnetic map $\mathbb{M}$, which is determined by the particle state $\mathbf{x}'$. The score function f takes three arguments $(\mathbf{b}_k, x', \mathbb{M})$, where the online measurement of the magnetic field $\mathbf{b}_k = [b^x, b^y, b^z]$, states of particles $\mathbf{x}'$ and magnetic field map $\mathbb{M}$. The transpose of the rotation matrix R^T is derived from the pose estimation and expressed as $R^T_x(\phi)R^T_y(\theta)R^T_z(\psi)$, which corresponds to each roll, pitch, and yaw.

As the last step, new samples X_k are drawn from the importance resampling performed by weights as follows:

$$p\left(X_k|Z_k, U_k\right) \approx \sum_{i=1}^{N} w_k^{[i]} \mathbf{x}_k^{[i]},$$

and the weight is normalized $w_k^{[i]} = 1/N$ via sequence importance resampling (SIR) [41], [42] and we then find the solution. For particles that have not arrived at the solution state, their weight is degraded in this feedback procedure. We refine the weight using physical constraints to provide more accurate predictions as a map matching. The state transition model (6) (human dynamics) can reflect the spatial constraints that an individual's movement process is sequential and that instantaneous movement is not possible as follows:

$$w_k := \begin{cases} 0 & d(\mathbf{o}'_k, \mathbf{c}_{\mathtt{NN}}) > \delta \\ w_k & d(\mathbf{o}'_k, \mathbf{c}_{\mathtt{NN}}) \leq \delta. \end{cases} \quad (12)$$

We use geomagnetic anomalies as a fingerprint to recover the heading direction via a recursive feedback loop in the resampling procedure. The geomagnetic field in the indoor environment is determined as a spatial map and is a stable feature over time. The anomalies of the flux vector are stored in the geomagnetic map $\mathbb{M}$ at the offline phase as *a priori* (learning) data. By learning the anomalies in three dimensions, the orientation of the smartphone can be determined in a coordinate system. The heading offset between the online magnetic field vector $\mathbf{b}$ and the offline training

This article has been accepted for publication in a future issue of this journal, but has not been fully edited. Content may change prior to final publication. Citation information: DOI 10.1109/ACCESS.2020.3029281, IEEE Access

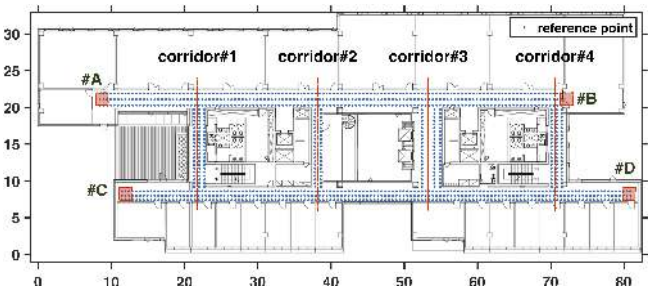

(a) corridor#1 (b) corridor#2 (c) corridor#3 (d) corridor#4

FIGURE 5. The floor plan at building N1. (1043 reference points)

data $\mathbb{M}$ is the heading offset, which should be calibrated, and provides the relative heading direction of the map. For global localization, the state of particles is initialized with a uniform distribution in all directions and locations, and the online magnetic field measurement is used to find the rotation matrix that is supposed to resemble $\mathbb{M}$.

IV. EVALUATION

A. EXPERIMENTAL ENVIRONMENT

We conducted extensive experiments on two buildings with different characteristics. The two buildings, N1 and KI, were built for research and as a large-scale auditorium, respectively. The building structure of N1 has roads that lead to several laboratories along the corridor. In constrast, building KI has an open space in the form of a large lobby with an auditorium in the center. Figs. 5 and 6 show the sizes of each the buildings in meters, which are approximately 83 m $\times$ 32 m and 65 m $\times$ 70 m, respectively.

For the offline phase in N1, learning data were obtained through the ML method. As shown in Fig. 5, 1043 reference points were preset with a floor plan at 50 cm intervals, and magnetic field states were recorded for 15 seconds on a smartphone mounted on a tripod at the corresponding location with zero inclination angle. The device aligned with the horizontal plane (paralleled to the ground plane) at the reference points. Since the location reference in N1 is a straight corridor structure, we attached yellow markers for guidance on the floor to distinguish the locations. When we calculated the total collection time of 1043 reference points, 4.35 hours (15,645 seconds) was required for building N1 deployment.

In KI, the WS method was used, and the path to which the starting and ending positions were determined was planned, as shown in Fig. 6. The interval between the paths was 60 cm, based on the size of the floor tiles. In the WS method, the datasets were collected in the usual scenario of walking while

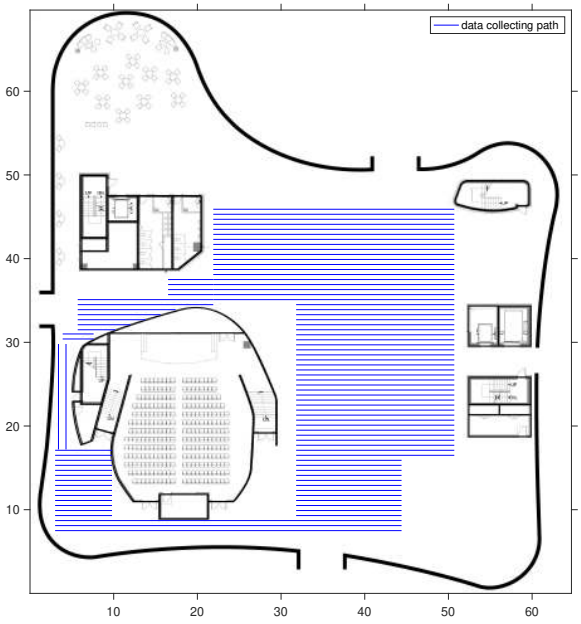

(a) The data collecting path.

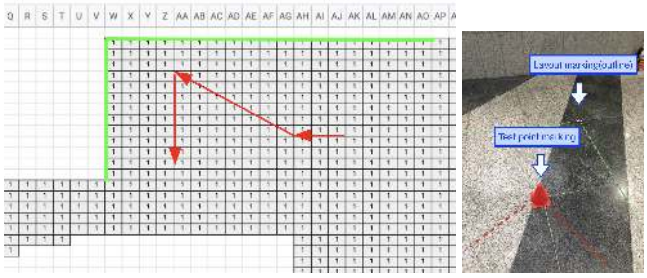

(b) An example of the test plan with floor tiles. (c) Markers for plan.

(d) A panoramic view in the open space.

FIGURE 6. The floor plan at building KI. (94 path lines)

holding a mobile phone without a stabilizing device such as a gimbal. The inclination of the phone, the angle between the screen and ground plane, was collected between about 0 degrees and 45 degrees to walk naturally. We placed colored cones in Fig. 6c to draw virtual lines for guidance on the start to the endpoint of paths. Through 94 paths gathered by the WS in building KI, 2337 reference points were created. The cumulative collection time was 0.38 hours (1372 seconds). The WS deployment took 0.59 seconds per reference point, 25x faster than the manual survey speed (15 seconds per reference). The difference in the actual labor intensity experienced was more substantial due to the structure of the building, location confirmation, and movement.

The test data were collected under identical conditions

This article has been accepted for publication in a future issue of this journal, but has not been fully edited. Content may change prior to final publication. Citation information: DOI 10.1109/ACCESS.2020.3029281, IEEE Access

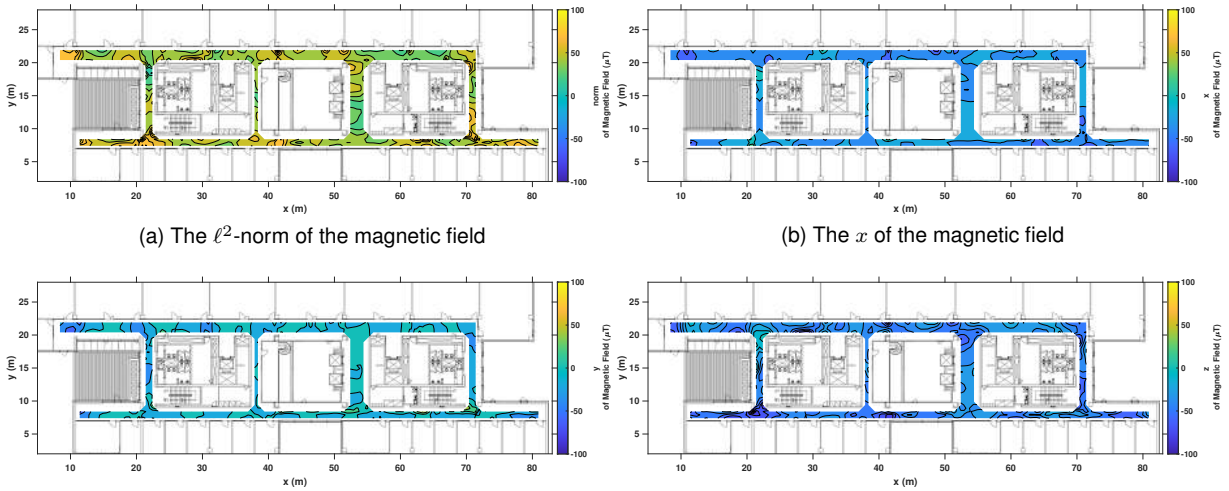

(a) The ℓ^2-norm of the magnetic field

(b) The x of the magnetic field

(c) The y of the magnetic field

(d) The z of the magnetic field

FIGURE 7. The magnetic field map for each component of the magnetic field vector in building N1.

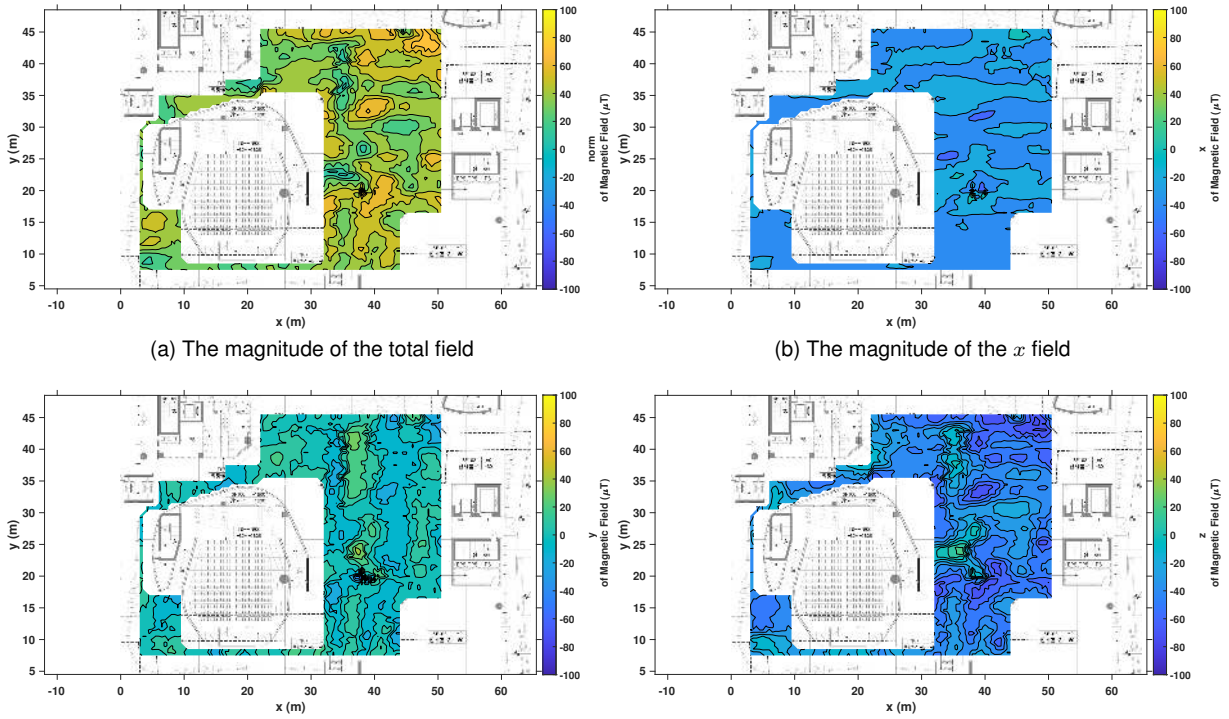

(a) The magnitude of the total field

(b) The magnitude of the x field

(c) The magnitude of the y field

(d) The magnitude of the z field

FIGURE 8. The magnetic field map for each component of the magnetic field vector in building KI.

to WS along the scenario's path. Five different models of smartphones were used for testing, which did not show a significant difference between the sensors of each manufacturer when calibrated [8], [11]. The models we used were Galaxy S8, S9 (Samsung Inc., with an Asahi Kasei Microdevices AK09916C magnetometer), iPhone X (Apple Inc), Nexus 6P (Google Inc., manufactured by Huawei, with a Bosch BMM150 3-axis magnetometer) and Mate 20 Pro (Huawei Inc.)

We compared MaLoc [43] as the state of the art utilizing VH components. Although MaLoc is not the latest research in magnetic field positioning, the reason for comparing MaLoc with ILoA is that we focus on the feature dimension of the magnetic field.

The path planning for fingerprint collection was set in a straight line with the start and endpoint in a manner similar to that of MaLoc [43]. However, we did not slice collecting path lines to shorten them. In MaLoc, coordinate labeling depends

This article has been accepted for publication in a future issue of this journal, but has not been fully edited. Content may change prior to final publication. Citation information: DOI 10.1109/ACCESS.2020.3029281, IEEE Access

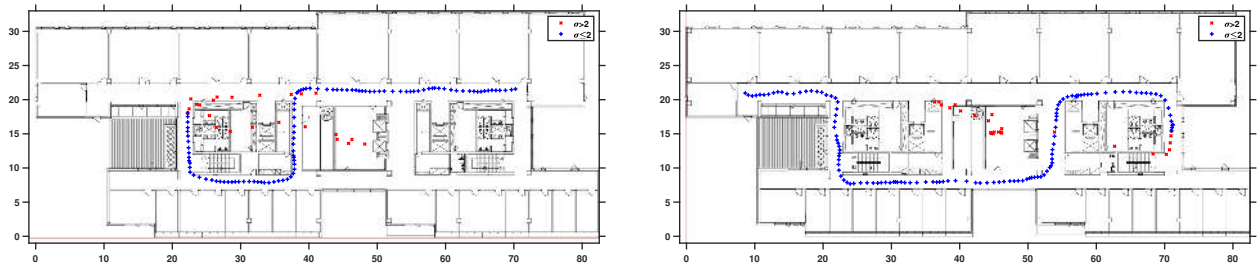

(a) A12B (b) D431A

FIGURE 9. Two sample results of test scenarios in N1.

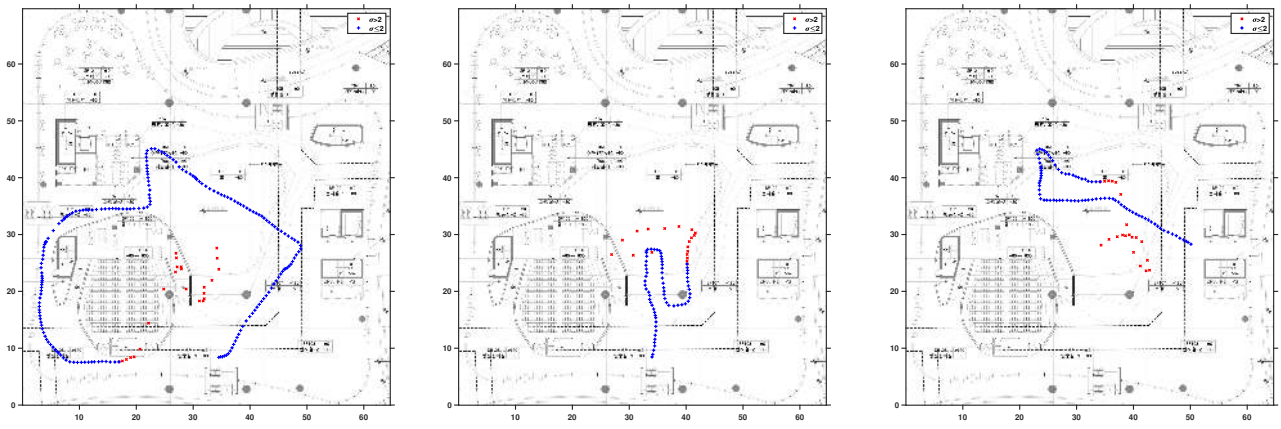

(a) Scenario 1 (b) Scenario 2 (c) Scenario 3

FIGURE 10. Three sample results of test scenarios in the KI.

on time, there is a constraint to walk at a constant speed, and it is likely to increase error over time. In ILoA, reference points are labeled according to a step event; it is unnecessary to have a constant speed, but a consistent stride length is assumed. We cannot ensure exactly consistent stride length keeps all time, but as the number of steps increases, the variation in stride length decreases. We corrected the magnetic field distortion that possibly caused by hard iron during each collecting path through the eight-motion calibration process.

For the test data collection in building KI, the open space was spacious, so there was no surrounding structure to refer to for the location, and the area was too large to place a marker on the floor. Therefore, path planning and coordinates were obtained by simulating the same number of tiles, as shown in Fig. 6b.

Figs. 7 and 8 depict the geomagnetic field (δ=0.8) in buildings N1 and KI. The contour plot's outline is the result obtained through the alpha shape, and ℓ^2-norm is, of course, a positive scalar value. Figs. 7d and 8d show that the variance of the z components is more prominent than that of x- or z-axis.

B. EVALUATION OF THE GLOBAL LOCALIZATION

We evaluated different path scenarios to analyze the global localization performance. Since the initial position probability of the particles was uniform over the entire area, it was possible to start at any position. We compared the trajectory by the convergence of the particles with the scenario as the ground truth. The precision rate was used to quantify global localization performance as the metric of consistency and reliability. To measure the convergence of particles, we used the *absolute deviation* (AD) of the statistical dispersion:

$$\begin{aligned} AD =& |x_k^{[i]} - m(X_k)| \\ \sigma_{AD} =& \sqrt{\frac{\sum_{i=1}^{N} \left(AD_k^i - \overline{AD}_k\right)^2}{N-1}}, \end{aligned} \tag{13}$$

where m is a mean function for the locations of particles.

The standard deviation of the AD (σ_{AD}) was used as a criterion to examine convergence. We defined true-positive (TP) and false-positive (FP) by whether the last half of the estimated trajectory converged on the ground truth and precision as TP/(TP+FP). We determined the threshold of the standard deviation for the convergence by the noise level ϵ in the transition model. The value of the threshold was chosen based on the following assumption: The standard deviation

This article has been accepted for publication in a future issue of this journal, but has not been fully edited. Content may change prior to final publication. Citation information: DOI 10.1109/ACCESS.2020.3029281, IEEE Access

should be less than the noise range when particles build a cluster (consensus), even though the particles spread with randomness in the state transition process.

Fig. 9 represents the estimated trajectories in building N1. The location results before convergence are denoted as red dots ('×'). The trajectories show that the initial phase's localization results are located around the center of the map. This is because the initial distribution of particles is uniform across all areas, and the estimated location (red dots) tends to appear at the center of the map by mean. The blue dots ('+') in Fig. 9 correspond to the localization results after convergence.

The letters A to D with the boxes marked are points to start or end. The red lines in Fig. 5 represent the identification number of corridors, which are passed through during testing. Therefore, the initial location and selection of corridors are chosen by randomness in the test scenarios. We can draw the collected pathway using the labels of each case. For example, 'D431A' in Fig. 9b means to start area is at D; go through corridors 4, 3, and 1; and then arrive at the end area A.

1) Effect of the Number of Particles

In building N1, we conducted the tests with 40 different path plans, and eight people participated in the test data collection. Both ILoA and MaLoc in Fig. 13b showed a precision rate close to 100% when they had a sufficient number of particles (N=2000 or more). In detail, the difference in convergence precision between the two methods in N1 was unclear due to correction by map matching. This is because the indoor space consisting of corridors has advantages in map matching that lead to a good effect.

In building KI, as it is an open space, we conducted tests with the three different path scenarios. Fig. 10 shows the estimated trajectories for each of the three scenarios. The first scenario starts at the south entrance, passes through a narrow corridor clockwise, reaches an open space, and returns to the south entrance. The second scenario starts at the east entrance and turns left heading to the south entrance, turns around to the north, then changes direction again and heads towards the south entrance. The third scenario starts at the north entrance, turns west, turns north-west, walks to the coffee shop's direction, turns south, and then proceeds diagonally to the east entrance.

In KI, when we compared the ILoA and MaLoc with the positioning performance, the proposed method showed a significant improvement in terms of precision. As shown in Figs. 13b and 14b, even if a sufficient number of particles (N=4000) were given, the convergence precision of MaLoc was 58%, whereas the best precision of ILoA was 98%. The results implicate that the VH features of MaLoc are constrained to pathway location on limited movement direction. In N1, although initial particles moved randomly in all directions, map constraints limit the physical movement of particles. For instance, the hallway structure leads particles into two directions. In KI, however, the weights of particles were not correctly updated with the direction-invariant feature. The feature ambiguity was not resolved with the VH components in the open space because of the low sensitivity in heading direction. Therefore, even if a sufficient number of particles are given, the global localization problem was not solved in open space. The weight of particles was assisted by map matching, and the weakness of low sensitivity in direction was not revealed.

2) Effect of the Augmented Geomagnetic Vector

We analyzed the impact of the direct-variant property in open space. Figs. 11 and 12 show the change of η with ILoA and MaLoc in KI in terms of the probability distribution over time. The probability distribution was expressed as color intensity, and the y-axis indicates the direction range $[0, 2\pi]$. η indicates the heading offset the sensor's body frame and the world reference frame, which augments the geomagnetic measurement. In initial phase, ground truths of η corresponding to each scenario are π, π, and $3\pi/2$. In Figs. 11 and 12, the initial heading is uniformly distributed over $[0, 2\pi]$ and then converging to the ground truths. The converged η gradually skews because it compensates for the drift error caused by the inertial sensor.

When we compared two groups, ILoA and MaLoc in Figs. 11 and 12, it showed a significant difference with the proceed of convergence results. In ILoA, the probability of η in Fig. 11 showed an aspect decreasing as the particles move away from the ground truth, which approximates a normal distribution. The results mean that the sensitivity of the direct-variant feature rewards the weights of particles with the heading variable. In contrast, the probability distribution in MaLoc was not related to the heading variable. The initial probabilities of particles in MaLoc were distributed in all directions, which was shown as clusters approximately uniform distribution. The direction-invariant property of VH features showed low sensitivity in terms of heading direction.

Table 1 summarizes the positioning error when we interpolate the geomagnetic map over the interval length δ. Best cases are chosen in each method by high precision first, and the cases are emphasized in bold font. The percentages of proposed method improvement over the MaLoc on building N1 and KI are 41% and 30% in terms of accuracy. The percentages of proposed method improvement are 0% and 40% in terms of precision.

In N1, the accuracy of ILoA improved by 6% and 9% for every 1000 particles added, and the accuracy of MaLoc improved by 7% and 4%. In terms of precision for every 1000 particles added, ILoA improved by 17% and 6%, and MaLoc improved by 22% and 1%. In KI, the accuracy of ILoA improved by 6% for 1000 particles added, and the MaLoc accuracy improved by 3%. In terms of precision for 1000 particle added, ILoA improved by 4% and 10%.

C. EVALUATION OF ACCURACY

We evaluated the accuracy of estimated location by the numerically computed error distance $\|x_{gt} - m(X_k)\|_2$, where x_{gt} is a test point location as a ground truth. The mean error

This article has been accepted for publication in a future issue of this journal, but has not been fully edited. Content may change prior to final publication. Citation information: DOI 10.1109/ACCESS.2020.3029281, IEEE Access

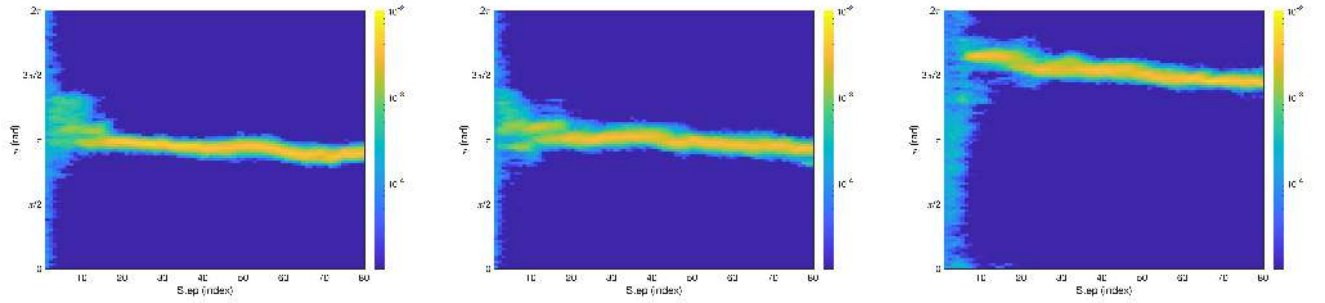

(a) Scenario 1 (b) Scenario 2 (c) Scenario 3

FIGURE 11. The ILoA heading offset (η) probability distribution with trajectories in building KI.

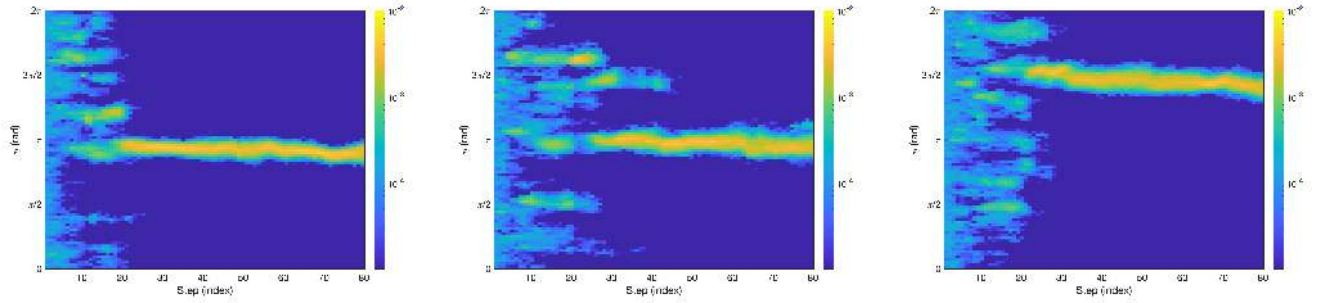

(a) Scenario 1 (b) Scenario 2 (c) Scenario 3

FIGURE 12. The MaLoc heading offset (η) probability distribution with trajectories in building KI.

TABLE 1. The summary of the result of accuracy with the level of interpolation granularity and the number of particles.

$\mathcal{B}^1$	$\mathcal{M}^2$	N^3 (x1000)	The interpolation granularity : δ (m) 0.1	0.2	0.3	0.5	0.8	1.0	1.2
			MED (m) / precision rate of convergence (%)						
N1	ILoA	1	0.48 / 74	0.54 / 85	0.56 / 78	0.55 / 81	0.49 / 77	0.62 / 88	0.66 / 76
		2	0.48 / 91	0.49 / 97	0.51 / 92	0.53 / 95	0.46 / 94	0.57 / 99	0.66 / 93
		3	0.45 / 99	0.48 / 99	0.47 / 100	0.47 / 100	**0.42 / 100**	0.55 / 100	0.65 / 100
	MaLoc	1	0.68 / 78	0.72 / 82	0.79 / 73	0.72 / 86	0.74 / 77	0.85 / 86	1.37 / 71
		2	0.69 / 100	0.64 / 97	0.68 / 95	0.70 / 100	0.69 / 99	0.83 / 97	1.36 / 57
		3	0.67 / 100	0.67 / 100	0.64 / 98	0.64 / 98	**0.66 / 100**	0.84 / 100	1.44 / 89
KI	ILoA	3	1.36 / 94	1.41 / 95	1.37 / 92	1.33 / 92	1.35 / 94	1.38 / 94	1.58 / 95
		4	1.29 / 96	1.41 / 96	1.25 / 93	1.29 / 95	1.34 / 97	**1.30 / 98**	1.55 / 98
	MaLoc	3	2.62 / 47	2.36 / 49	2.66 / 48	2.22 / 48	2.30 / 49	1.95 / 48	2.46 / 51
		4	2.26 / 52	2.57 / 50	2.74 / 50	2.12 / 54	2.32 / 55	**1.81 / 58**	2.50 / 51

[1] Building [2] Methodology [3] Number of particles

distance (MED) was used as the error metric of accuracy, and MED determined the performance of positioning.

1) Effect of the Interpolation

Figs. 13a and 14a show the positioning accuracy according to the number of particles and interpolation granularity. In N1, Fig. 14a shows that the accuracy attained the inflection point of the curve at $\delta = 0.8$. However, in building KI, the results of which are in Fig. 14a, the inflection point seems to be unclear due to the overall positioning performance degradation resulting from the open space.

The optimal δ of the geomagnetic map seems to be related to the step length converted from the online phase's observation sampling rate. Ideally, in importance sampling, particle weights should be well estimated in the update process. We suppose that the ideal granularity of the geomagnetic map is tied to the online sampling rate, which conforms with *human gait*. This is because the magnetometer sampling rate is faster than the human gait. Therefore, the resolution of the geomagnetic map should be higher than the stride length to

This article has been accepted for publication in a future issue of this journal, but has not been fully edited. Content may change prior to final publication. Citation information: DOI 10.1109/ACCESS.2020.3029281, IEEE Access

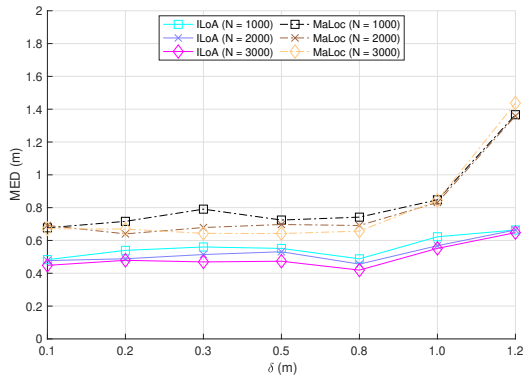

(a) MED with δ and N particles.

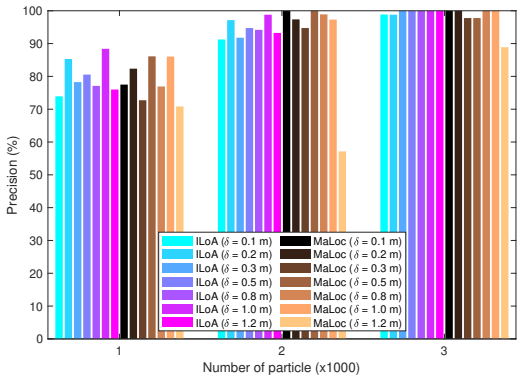

(b) The precision rate with δ and N particles.

FIGURE 13. The mean error distance and precision rate in building N1.

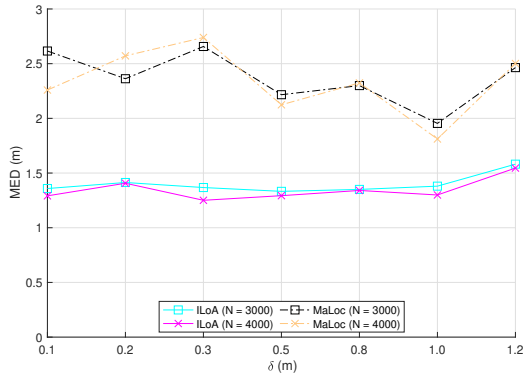

(a) MED with δ and N particles.

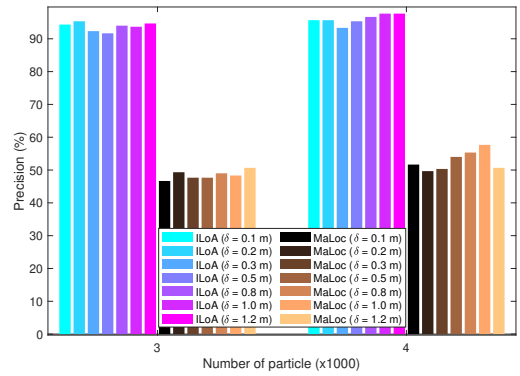

(b) The precision rate with δ and N particles.

FIGURE 14. The mean error distance and precision rate in building KI.

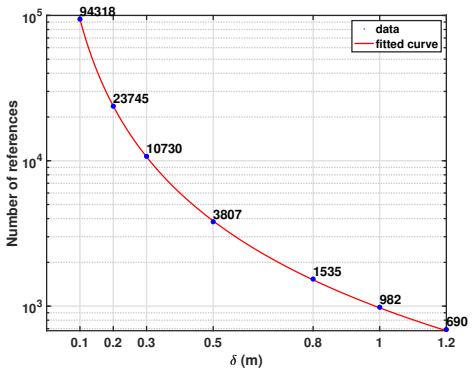

FIGURE 15. The size of the search space with the magnetic map granularity.

cover the distance that moved during the sampling period.

An overly fine-grained geomagnetic map limits localization performance contrariwise because it increases the likelihood of overfitting and increases ambiguity in the search space. This is because the online measurement resolution relies on the step speed/frequency, and the high resolution of $\mathbb{M}$ increases the complexity $\mathcal{O}(|\mathbb{M}|)$ and ambiguity with the enlarged search space.

We formalize the growth rate by the δ parameter to analyze the computational complexity of localization in the online phase. δ is inversely proportional to the density of the reference point in a space, which corresponds to the $\mathcal{O}(n^2)$ and $n \propto 1/\delta$. Fig. 15 displays the number of references with the δ parameter. The fitted curve equation is $a * \delta^b$, where a is 972.9 and b is -1.987. (R-squared: 1, RMSE: 54.55)

2) Effect of the Attitude

We conducted an additional experiment for attitude analysis because each person has a different attitude, even in a typical walking motion. Each line of the Fig. 16 shows an aspect of the magnetic field change with different attitudes, inclination angles, and walking about 60 meters (sampling rate=50Hz). We determined the attitude as the pitch angle between the screen facing and the ground plane. Each column denotes the change of ℓ^2-norm, three components of the magnetic field, and the calibrated result. The norm is a direction invariant scalar, so there were no evident difference for each attitude. When the patterns are decomposed into three-axis

This article has been accepted for publication in a future issue of this journal, but has not been fully edited. Content may change prior to final publication. Citation information: DOI 10.1109/ACCESS.2020.3029281, IEEE Access

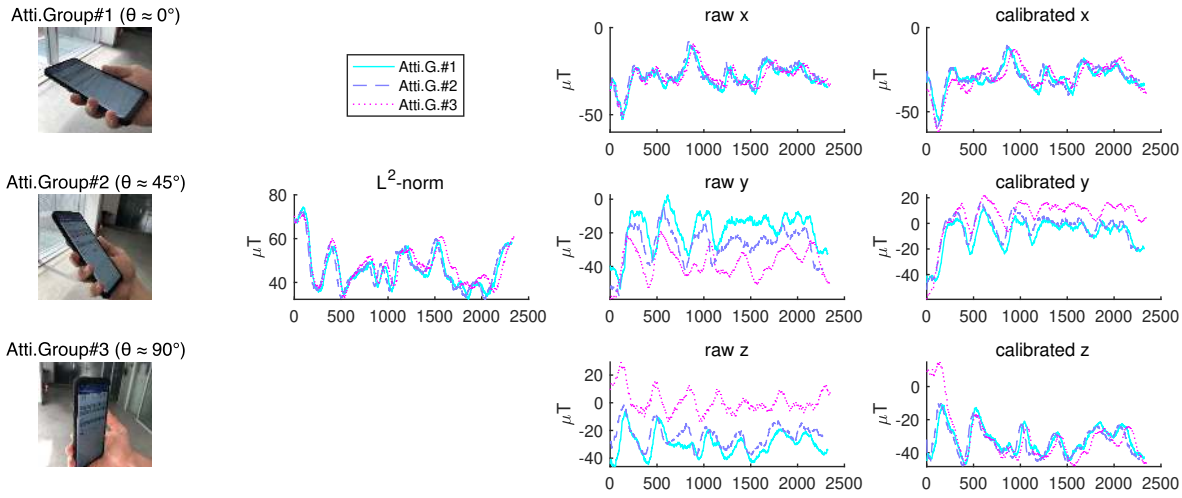

FIGURE 16. The geomagnetic patterns while walking 60 meters with different attitudes, and their calibrated results.

magnetic field details, it showed differences. However, when we calibrated the vectors, a similar pattern was reproduced by tilt correction.

V. DISCUSSION

In this section, we discuss the details that are not covered in this paper. In future work, we will consider the following improvements.

A. DEGENERACY AND IMPOVERISHMENT

The performance of the localization can be inferred by evaluating the position error. Additionally, we want to refer to the convergence rate of particles as a qualitative precision analysis. In somewhat detailed aspects, heuristic values such as noise distributions over the modeling are crucial to convergence, but we do not address why we set that exact value because it was not taken systematically. The fundamental difficulties [44] associated with particle filters are degeneracy and impoverishment of the particle samples. These problems are commonly associated with the distribution of particles because the weight of the particles is not appropriately distributed. The regularization [45] technique can improve the performance of the particle filter, but parameters have a delicate impact on particle distribution and performance. We strive to reduce the effect of these parameters to help prevent overfitting via the SIR approach, but there remain interesting details to be addressed.

B. AUTOMATE MAP GENERATION

The magnetic field map requires sufficient reference points because the necessary granularity is high. Therefore, if individuals need to manually collect data on a reference point and move directly on the floor plan, the process is labor intensive and exhibits poor scalability. In terms of scalability, mobile robots are useful applications. The SLAM in the robotics field is an applicable technique for solving the cost of indoor map calibration [46]. Mobile robots can reduce the cost of collection and increase the accuracy of maps. Vacuum cleaning robots, which are becoming increasingly common in homes, are equipped with high-precision distance sensors based on LiDAR.

C. SIMILARITY FUNCTION

Euclidean distance is an intuitive and straightforward approach to measure similarity. However, in vector space, *cosine similarity* is likely to yield better results. Therefore, we also tested other similarity measures, including the cosine similarity measure. We found that Euclidean distance exhibited the best performance when compared to the other similarity functions. The analysis of these results suggests the importance of magnitude, as well as orientation. The range (image) of the cosine similarity function f according to the cosine function is limited to [0, 1]. Nonetheless, more research is needed to improve this aspect through a more sophisticated model than the Euclidean similarity function.

VI. CONCLUSION

In this paper, we have proposed a novel localization method to construct the three-axis geomagnetic anomaly map and utilized it. The effectiveness of the augmented geomagnetic vector was demonstrated in a variety of path scenarios by solving the global localization problem. We analyzed the effect of the direction-variant feature for heading estimation, which resolves the directional ambiguity. Furthermore, we validated our approach and presented promising results in an open space environment, where no map information to aid in localization such as map matching. The proposed method can be easily extended to incorporate other sensors as well as applicable to most mobile devices. We expect that incorporating visual pose measurements could improve its attitude robustness.

REFERENCES

[1] P. Bahl and V. N. Padmanabhan, "Radar: an in-building rf-based user location and tracking system," in *Proceedings IEEE INFOCOM 2000. Conference on Computer Communications. Nineteenth Annual Joint Conference of the IEEE Computer and Communications Societies (Cat. No.00CH37064)*, vol. 2, 2000, pp. 775–784 vol.2.

[2] R. Mautz, *Indoor Positioning Technologies*, ser. Geodätisch-geophysikalische Arbeiten in der Schweiz. ETH Zurich, Department of Civil, Environmental and Geomatic Engineering, Institute of Geodesy and Photogrammetry, 2012. [Online]. Available: https://books.google.co.kr/books?id=BsHpMgEACAAJ

[3] E. Martin, O. Vinyals, G. Friedland, and R. Bajcsy, "Precise indoor localization using smart phones," in *Proceedings of the 18th ACM International Conference on Multimedia*, ser. MM '10. New York, NY, USA: ACM, 2010, pp. 787–790. [Online]. Available: http://doi.acm.org/10.1145/1873951.1874078

[4] P. D. Groves, *Principles of GNSS, inertial, and multisensor integrated navigation systems*. Artech house, 2013.

[5] S. Qiu, Z. Wang, H. Zhao, K. Qin, Z. Li, and H. Hu, "Inertial/magnetic sensors based pedestrian dead reckoning by means of multi-sensor fusion," *Information Fusion*, vol. 39, pp. 108–119, 2018.

[6] A. Xiao, R. Chen, D. Li, Y. Chen, and D. Wu, "An indoor positioning system based on static objects in large indoor scenes by using smartphone cameras," *Sensors*, vol. 18, p. 2229, 07 2018.

[7] Z. Chen, H. Zou, H. Jiang, Q. Zhu, Y. C. Soh, and L. Xie, "Fusion of wifi, smartphone sensors and landmarks using the kalman filter for indoor localization," *Sensors*, vol. 15, no. 1, pp. 715–732, 2015.

[8] Y. Shu, C. Bo, G. Shen, C. Zhao, L. Li, and F. Zhao, "Magicol: Indoor localization using pervasive magnetic field and opportunistic wifi sensing," *IEEE Journal on Selected Areas in Communications*, vol. 33, no. 7, pp. 1443–1457, 2015.

[9] H. C. Ockerse, J. H. Bechtel, and M. D. Bugno, "Electronic compass system," Aug. 9 2005, uS Patent 6,928,366.

[10] B. Li, T. Gallagher, A. G. Dempster, and C. Rizos, "How feasible is the use of magnetic field alone for indoor positioning?" in *2012 International Conference on Indoor Positioning and Indoor Navigation (IPIN)*, Nov 2012, pp. 1–9.

[11] K. pathapati subbu, B. Gozick, and R. Dantu, "Locateme: Magnetic-fields-based indoor localization using smartphones," *ACM Transactions on Intelligent Systems and Technology (TIST)*, vol. 4, 09 2013.

[12] S. Song, C. Hu, M. Li, W. Yang, and M. Q.-H. Meng, "Real time algorithm for magnet's localization in capsule endoscope," in *2009 IEEE International Conference on Automation and Logistics*. IEEE, 2009, pp. 2030–2035.

[13] J. Blankenbach and A. Norrdine, "Position estimation using artificial generated magnetic fields," in *2010 International Conference on Indoor Positioning and Indoor Navigation*. IEEE, 2010, pp. 1–5.

[14] D. Arumugam, J. Griffin, D. Stancil, and D. Ricketts, "Higher order loop corrections for short range magnetoquasistatic position tracking," in *2011 IEEE International Symposium on Antennas and Propagation (APSURSI)*. IEEE, 2011, pp. 1755–1757.

[15] M. Hehn, E. Sippel, C. Carlowitz, and M. Vossiek, "High-Accuracy Localization and Calibration for 5-DoF Indoor Magnetic Positioning Systems," *IEEE Transactions on Instrumentation and Measurement*, vol. 68, no. 10, pp. 4135–4145, 2019.

[16] J. Chung, M. Donahoe, C. Schmandt, I.-J. Kim, P. Razavai, and M. Wiseman, "Indoor location sensing using geo-magnetism," in *Proceedings of the 9th international conference on Mobile systems, applications, and services*. ACM, 2011, pp. 141–154.

[17] A. Bilke and J. Sieck, "Using the magnetic field for indoor localisation on a mobile phone," in *Progress in Location-Based Services*. Springer, 2013, pp. 195–208.

[18] M. H. Afzal, V. Renaudin, and G. Lachapelle, "Magnetic field based heading estimation for pedestrian navigation environments," in *Indoor Positioning and Indoor Navigation (IPIN), 2011 International Conference on*. IEEE, 2011, pp. 1–10.

[19] B. Gozick, K. P. Subbu, R. Dantu, and T. Maeshiro, "Magnetic maps for indoor navigation," *IEEE Transactions on Instrumentation and Measurement*, vol. 60, no. 12, pp. 3883–3891, Dec 2011.

[20] W. Storms, J. Shockley, and J. Raquet, "Magnetic field navigation in an indoor environment," in *2010 Ubiquitous Positioning Indoor Navigation and Location Based Service*, Oct 2010, pp. 1–10.

[21] W. Shao, F. Zhao, C. Wang, H. Luo, M. Tunio, Q. Wang, and D. li, "Location fingerprint extraction for magnetic field magnitude based indoor positioning," *Journal of Sensors*, vol. 2016, pp. 1–16, 01 2016.

[22] Seong-Eun Kim, Yong Kim, Jihyun Yoon, and Eung Sun Kim, "Indoor positioning system using geomagnetic anomalies for smartphones," in *2012 International Conference on Indoor Positioning and Indoor Navigation (IPIN)*, Nov 2012, pp. 1–5.

[23] M. McCaig, *Permanent magnets in theory and practice / Malcolm McCaig*. Pentech Press London, 1977.

[24] H. Xie, T. Gu, X. Tao, H. Ye, and J. Lv, "Maloc: A practical magnetic fingerprinting approach to indoor localization using smartphones," in *Proceedings of the 2014 ACM International Joint Conference on Pervasive and Ubiquitous Computing*, ser. UbiComp '14. New York, NY, USA: ACM, 2014, pp. 243–253. [Online]. Available: http://doi.acm.org/10.1145/2632048.2632057

[25] H.-S. Kim, W. Seo, and K.-R. Baek, "Indoor positioning system using magnetic field map navigation and an encoder system," *Sensors*, vol. 17, no. 3, p. 651, 2017.

[26] H. J. Jang, J. M. Shin, and L. Choi, "Geomagnetic field based indoor localization using recurrent neural networks," in *GLOBECOM 2017 - 2017 IEEE Global Communications Conference*, Dec 2017, pp. 1–6.

[27] H. J. Bae and L. Choi, "Large-scale indoor positioning using geomagnetic field with deep neural networks," in *ICC 2019 - 2019 IEEE International Conference on Communications (ICC)*, May 2019, pp. 1–6.

[28] X. Wang, Z. Yu, and S. Mao, "Deepml: Deep lstm for indoor localization with smartphone magnetic and light sensors," in *2018 IEEE International Conference on Communications (ICC)*, May 2018, pp. 1–6.

[29] I. Ashraf, M. Kang, S. Hur, and Y. Park, "MINLOC:Magnetic Field Patterns-Based Indoor Localization Using Convolutional Neural Networks," *IEEE Access*, vol. 8, pp. 66 213–66 227, 2020.

[30] H. Edelsbrunner and E. P. Mücke, "Three-dimensional alpha shapes," *ACM Trans. Graph.*, vol. 13, no. 1, pp. 43–72, Jan. 1994. [Online]. Available: http://doi.acm.org/10.1145/174462.156635

[31] A. Bowyer, "Computing dirichlet tesselations," *Comput. J.*, vol. 24, pp. 162–166, 02 1981.

[32] H. Edelsbrunner, D. Kirkpatrick, and R. Seidel, "On the shape of a set of points in the plane," *IEEE Transactions on Information Theory*, vol. 29, no. 4, pp. 551–559, July 1983.

[33] S. Thompson, "Indooratlas," *Online]: http://www. indooratlas. com*.

[34] S. O. H. Madgwick, A. J. L. Harrison, and R. Vaidyanathan, "Estimation of imu and marg orientation using a gradient descent algorithm," in *2011 IEEE International Conference on Rehabilitation Robotics*, June 2011, pp. 1–7.

[35] B. Khaleghi, A. Khamis, F. O. Karray, and S. N. Razavi, "Multisensor data fusion: A review of the state-of-the-art," *Inf. Fusion*, vol. 14, no. 1, pp. 28–44, Jan. 2013. [Online]. Available: http://dx.doi.org/10.1016/j.inffus.2011.08.001

[36] Q. Gan and C. J. Harris, "Comparison of two measurement fusion methods for kalman-filter-based multisensor data fusion," *IEEE Transactions on Aerospace and Electronic Systems*, vol. 37, no. 1, pp. 273–279, Jan 2001.

[37] D. Smith and S. Singh, "Approaches to multisensor data fusion in target tracking: A survey," *IEEE Transactions on Knowledge and Data Engineering*, vol. 18, no. 12, pp. 1696–1710, Dec 2006.

[38] V. Fox, J. Hightower, , D. Schulz, and G. Borriello, "Bayesian filtering for location estimation," *IEEE Pervasive Computing*, vol. 2, no. 3, pp. 24–33, July 2003.

[39] Z. Chen, "Bayesian filtering: From kalman filters to particle filters, and beyond," *Statistics*, vol. 182, 01 2003.

[40] I. Nygren, "Robust and efficient terrain navigation of underwater vehicles," in *2008 IEEE/ION Position, Location and Navigation Symposium*, May 2008, pp. 923–932.

[41] A. Doucet, S. Godsill, and C. Andrieu, "On sequential monte carlo sampling methods for bayesian filtering," *Statistics and Computing*, vol. 10, no. 3, pp. 197–208, Jul 2000. [Online]. Available: https://doi.org/10.1023/A:1008935410038

[42] J. S. Liu and R. Chen, "Sequential monte carlo methods for dynamic systems," *Journal of the American Statistical Association*, vol. 93, no. 443, pp. 1032–1044, 1998. [Online]. Available: https://doi.org/10.1080/01621459.1998.10473765

[43] H. Xie, T. Gu, X. Tao, H. Ye, and J. Lu, "A reliability-augmented particle filter for magnetic fingerprinting based indoor localization on smartphone," *IEEE Transactions on Mobile Computing*, vol. 15, no. 8, pp. 1877–1892, Aug. 2016. [Online]. Available: doi.ieeecomputersociety.org/10.1109/TMC.2015.2480064

[44] T. Li, S. Sun, T. P. Sattar, and J. M. Corchado, "Review: Fight sample degeneracy and impoverishment in particle filters: A review of intelligent approaches," *Expert Syst. Appl.*, vol. 41, no. 8, pp. 3944–3954, Jun. 2014. [Online]. Available: http://dx.doi.org/10.1016/j.eswa.2013.12.031

[45] F. Campillo and V. Rossi, "Convolution particle filter for parameter estimation in general state-space models," *IEEE Transactions on Aerospace and Electronic Systems*, vol. 45, no. 3, pp. 1063–1072, July 2009.

[46] S. Lee, N. Lee, J. Ahn, J. Kim, B. Moon, S. Jung, and D. Han, "Construction of an indoor positioning system for home iot applications," in *2017 IEEE International Conference on Communications (ICC)*, May 2017, pp. 1–7.

SANGJAE LEE received his M.S. in Computer Science from the Korea Advanced Institute of Science and Technology (KAIST), Daejeon, Korea. He is currently working toward a Ph.D. at the School of Computing, KAIST. His research interests include machine learning, mobile sensor technologies, computer vision, and indoor positioning.

SEUNGWOO CHAE received his M.S. in Computer Science from the Korea Advanced Institute of Science and Technology (KAIST), Daejeon, Korea. He is currently working toward a Ph.D. at the School of Computing, KAIST. His research interests include deep learning for indoor positioning and tracking on handheld devices, mobile sensor technologies, and sensor fusion.

DONGSOO HAN received his PhD in information science from Kyoto University. He is a professor of computer science at the Korea Advanced Institute of Science and Technology (KAIST). He is also a director at the Indoor Positioning Research Center, KAIST. His research interests include indoor positioning, pervasive computing, and location-based mobile applications. He is a member of IEEE.